Mon. Not. R. Astron. Soc. **388,** 1775–1786 (2008) doi:10.1111/j.1365-2966.2008.13515.x

Radio source calibration for the Very Small Array and other cosmic microwave background instruments at around 30 GHz

Yaser A. Hafez,[1,2⋆] Rod D. Davies,[2⋆] Richard J. Davis,[2⋆] Clive Dickinson,[3] Elia S. Battistelli,[4,5] Francisco Blanco,[2] Kieran Cleary,[6] Thomas Franzen,[7] Ricardo Genova-Santos,[4] Keith Grainge,[7] Michael P. Hobson,[7] Michael E. Jones,[8] Katy Lancaster,[9] Anthony N. Lasenby,[7] Carmen P. Padilla-Torres,[4] José Alberto Rubiño-Martin,[4] Rafael Rebolo,[4] Richard D. E. Saunders,[7] Paul F. Scott,[7] Angela C. Taylor,[8] David Titterington,[7] Marco Tucci[4] and Robert A. Watson[2]

[1]*National Centre for Mathematics and Physics, KACST, PO Box 6086, Riyadh 11442, Saudi Arabia*
[2]*Jodrell Bank Centre for Astrophysics, The University of Manchester, Manchester M13 9PL*
[3]*Infrared Processing and Analysis Center, California Institute of Technology, M/S 220-6, 1200 E. California Blvd., Pasadena, CA 91125, USA*
[4]*Instituto de Astrofisíca de Canarias, 38200 La Laguna, Tenerife, Canary Islands, Spain*
[5]*Department of Physics & Astronomy, University of British Columbia, 6224 Agricultural Road, Vancouver, British Columbia, Canada V6T 1Z1*
[6]*California Institute of Technology, M/S 105-24, 1200 E. California Blvd., Pasadena, CA 91125, USA*
[7]*Astrophysics Group, Cavendish Laboratory, University of Cambridge, Madingley Road, Cambridge CB3 0HE*
[8]*Astrophysics Group, Denys Wilkinson Building, University of Oxford, Keeble Road, Oxford OX1 3RH*
[9]*H. H. Wills Physics Laboratory, University of Bristol, Tyndall Avenue, Bristol BS8 1TL*

Accepted 2008 May 26. Received 2008 May 23; in original form 2008 April 18

ABSTRACT

Accurate calibration of data is essential for the current generation of cosmic microwave background (CMB) experiments. Using data from the Very Small Array (VSA), we describe procedures which will lead to an accuracy of 1 per cent or better for experiments such as the VSA and CBI. Particular attention is paid to the stability of the receiver systems, the quality of the site and frequent observations of reference sources. At 30 GHz the careful correction for atmospheric emission and absorption is shown to be essential for achieving 1 per cent precision.

The sources for which a 1 per cent relative flux density calibration was achieved included Cas A, Cyg A, Tau A and NGC 7027 and the planets Venus, Jupiter and Saturn. A flux density, or brightness temperature in the case of the planets, was derived at 33 GHz relative to Jupiter which was adopted as the fundamental calibrator. A spectral index at ∼30 GHz is given for each.

Cas A, Tau A, NGC 7027 and Venus were examined for variability. Cas A was found to be decreasing at 0.394 ± 0.019 per cent yr^{-1} over the period 2001 March to 2004 August. In the same period Tau A was decreasing at 0.22 ± 0.07 per cent yr^{-1}. A survey of the published data showed that the planetary nebula NGC 7027 decreased at 0.16 ± 0.04 per cent yr^{-1} over the period 1967–2003. Venus showed an insignificant (1.5 ± 1.3 per cent) variation with Venusian illumination. The integrated polarization of Tau A at 33 GHz was found to be 7.8 ± 0.6 per cent at position angle $=148^\circ \pm 3^\circ$.

Key words: methods: observational – techniques: interferometric – cosmic microwave background – cosmology: observations – radio continuum: ISM – radio continuum: Solar system.

1 INTRODUCTION

With the increasing sensitivity of cosmic microwave background (CMB) experiments, it is important to have accurate calibration of the intensity or temperature scale of each experiment. The

⋆E-mail: yhafez@kacst.edu.sa (YAH); rdd@jb.man.ac.uk (RDD); rjd@jb.man.ac.uk (RJD)

cosmological significance of the data is directly dependent on this scale. For example, the amplitude of the first peak in the CMB power spectrum is proportional to Ω_b while the ratio of the first to the third peak, derived from a mix of experiments probing different angular modes ℓ, is also sensitive to Ω_b. Furthermore, the fractional uncertainty in the power spectrum is twice that of the fractional uncertainty in the temperature scale. Current CMB experiments would greatly benefit from a coherent calibration across experiments such as *Planck*, *Wilkinson Microwave Anisotropy Probe* (*WMAP*), Cosmic Background Imager (CBI), Very Small Array (VSA), etc. at an accuracy of 1 per cent or better. The present investigation provides a set of source intensities calibrated to this precision at a frequency of 33 GHz.

We have chosen the brightest planets and strongest radio sources to calibrate the VSA on a frequent (typically few hours) basis during CMB observations. The basic calibration of all the targets used in the VSA is in terms of an assumed brightness temperature of Jupiter (Watson et al. 2003; Dickinson et al. 2004), which in turn, is tied to the CMB dipole (Hinshaw et al. 2008).

Inevitably the strongest sources used for the frequent calibration of VSA data are sufficiently extended (a few arcmin) that their total flux densities require correction when applied to the ∼10 arcmin resolution of the VSA at an accuracy of better than 1 per cent. Cas A, Tau A and Cyg A fall into this category although for Cyg A the effect is ≤ 0.3 per cent. The planets do not require such a correction.

The polarization of the calibrators also needs to be taken into account. The most strongly polarized source is Tau A. The integrated emission from H II regions and the planets are not expected to be polarized. The radial polarization of the planets would only be of concern if there were a significant phase effect in the brightness distribution across the planet.

Time variability is an important consideration when using calibrators. Many of the stronger extragalactic sources such as quasars have to be rejected for this reason. This is an integral part of the present study.

The spectral index of a calibrator needs to be specified if the calibration process is to be useful between experiments which have different central frequencies and bandwidths even within the 1 cm wavelength band investigated here. In general, spectral index data are taken from the literature.

The main challenge in accurate calibration of ground-based observations at centimetric and millimetric frequencies is provided by the atmosphere. A high dry site is a pre-requisite. The Izaña observatory of the IAC has a proven record of observations in the range 10–33 GHz (Davies et al. 1996). An assessment of its properties at these frequencies will be given in a separate paper (Davies et al., in preparation).

This paper is arranged as follows. Section 2 describes the relevant features of the VSA used in this investigation. The philosophy of the approach, including the method of determining the atmospheric corrections, is given in Section 3. The results given as flux densities, or brightness temperatures[1] in the case of the planets, are presented along with the adopted spectral indices in Section 4, which also includes a discussion of source variability and polarization. The conclusions of this paper are summarized in Section 5.

[1] All planetary temperatures discussed in this paper are the Rayleigh–Jeans brightness temperature minus the Rayleigh–Jeans temperature of the CMB at the same frequency.

2 THE VSA AND ITS CALIBRATION SYSTEM

The advantage of using an interferometer for 'point-source' flux density measurements is that the extended emission from the sky, atmosphere and the ground can be largely eliminated. The VSA is described in detail by Scott et al. (2003), Watson et al. (2003) and Dickinson et al. (2004). A summary of its main features is now given.

2.1 The overall system

The VSA is a 14-element interferometer operating in the Ka band (26–36 GHz). It is located on the high and dry site at the Teide Observatory, Izaña, Tenerife, at an altitude of 2340 m. The antenna of each element consists of a conical corrugated horn feeding a paraboloidal mirror. Each antenna and its associated cryogenically cooled receiver system can be placed anywhere on a 4×3 m^2 tip-tilt table located in a metal enclosure to minimize any emission contribution from the ground. Due to the geometry of the table and the enclosure, the VSA declination (Dec.) is restricted to the range -5° to $+60^\circ$. Tracking of a field is accomplished by a combination of table tilt and rotation of each mirror.

Since the beginning of CMB observations in 2000 September the VSA has been operated in both a compact and extended configuration. In the compact configuration the mirror diameters were 143 mm giving a primary beamwidth (FWHP) of 4.°6. The geometrical arrangement of the antennas on the table gave interferometer baseline lengths ranging from 0.20 to 1.23 m allowing angular multipoles of $l = 150$–900 to be probed at the observing frequency of 34.1 GHz. The resolution of the array was ∼17 arcmin depending on the field Dec. and hour angle range observed.

The extended array, which became operational in 2001 October, used an antenna configuration which covered a baseline range of 0.6–2.5 m thereby extending the range of angular multipoles to $l = 1500$ and gave a synthesized beamwidth (FWHP) of ∼11 arcmin. The larger mirror diameters provided a factor of 1.6 improvement in filling factor and an overall factor of ∼3 in temperature sensitivity (see Table 1). Since 2005 September the VSA has operated in a third configuration, the superextended array, with 60-cm aperture mirrors (Genova-Santos et al. 2008).

The VSA has operated at either 33 or 34.1 GHz with an instantaneous bandwidth of 1.5 GHz. With an average system temperature of some 35 K the VSA achieves an overall instantaneous point-source sensitivity of ≈36 and 6 Jy s$^{1/2}$ in the compact and extended

Table 1. Specification of the VSA in the compact and extended configurations.

	Compact	Extended
Dec. range	−5 to +60	−5 to +60
Number of antennas (baselines)	14(91)	14(91)
Range of baseline lengths	0.20–1.23 m	0.6–2.5 m
Centre frequencies	34 GHz	33, 34 GHz
Bandwidth of observation	1.5 GHz	1.5 GHz
System temperature, T_{sys}	≈35 K	≈35 K
Mirror diameters	143 mm	332 mm
Primary beam (FWHM)	4.°6	2.°0
Synthesized beam (FWHM)	≈17 arcmin	≈11 arcmin
Range of angular multipole (l)	150 to 900	300 to 1500
Point-source sensitivity	≈36 Jy s$^{1/2}$	≈6 Jy s$^{1/2}$
Temperature sensitivity per beam	≈40 mK s$^{1/2}$	≈15 mK s$^{1/2}$
Polarization	Linear (vertical)	Linear (vertical)

configurations, respectively; the corresponding temperature sensitivities are 40 and 15 mK $s^{1/2}$. The VSA is linearly polarized in the vertical direction and is therefore sensitive to any linear polarization in the calibration sources.

2.2 Present analysis

An interferometer array like the VSA requires an accurate determination of the position of the antennas to produce reliable relative observations at the 1 per cent level aimed at in this paper. A maximum likelihood technique has been applied to the calibrator source observations in order to constrain such telescope parameters as the antenna positions, effective observing frequencies and correlator amplitudes and phase shifts (Maisinger et al. 2003). The stability of the VSA is such that these calibration observations are required only every few hours.

The overall gain of each antenna is monitored continuously by means of a noise-injection system. A modulated noise signal is injected into each antenna via a probe in the horn and is measured using phase-sensitive detection after the automatic gain control (AGC) stage in the intermediate frequency system. The relative contribution of the constant noise source to the total output power from each antenna varies inversely with system temperature and thus a correction can be made to the overall flux calibration. This system allows account to be taken of the gain and variations in total set noise due, for example, to atmospheric emission. It potentially provides an indication of weather conditions and is a primary indicator for flagging weather-affected data in CMB observations. In the face of the stringent requirements here of better than 1 per cent calibration accuracy, this approach had to be modified as described in the next section.

3 THE SOURCE CALIBRATION PROGRAMME

We consider here the methods used to measure relative flux densities to an accuracy of 1 per cent or better at frequencies around 30 GHz.

3.1 Calibration sources for CMB observations

The sources available for this study are those bright enough to be detected with good signal-to-noise ratio in say 20 min of observing time. This limits them to ≥ 10 Jy in the two configurations, which allows the following sources to be used as primary calibrators: Tau A, Cas A, Cyg A, Jupiter, Saturn and Venus. Observations on these sources of 10–30 min are interleaved within CMB fields. These observations provide the data archive on which the present investigation is based. Additional long-track observations covering $\pm$ 3 h in hour angle were used to quantify elevation-dependent atmospheric effects.

3.2 Data reduction procedures

The basic data reduction of VSA data followed the same procedure as described in early VSA work (e.g. Taylor et al. 2003; Dickinson et al. 2004). One radio source (or the CMB) is calibrated against another (the 'calibrator') by converting the units of the 91 raw visibilities from correlator units to flux densities via the primary 'calibrator' for each baseline and then combining them to give a mean flux density for the source. The resulting 91 baseline visibility tracks are checked by eye and interactively searched for residual contaminating signals. Due to the large number of calibrator observations we were able to be fastidious about data quality. Some 20 per cent of the data are removed in this way in addition to the more obvious errors due to hardware failure and bad weather. The elevation of each source was recorded and could be used to make subsequent corrections for atmospheric effects.

3.3 Choice of fundamental reference source

The flux calibration of VSA data is tied to observations of Jupiter which is widely used as a calibrator for CMB observations in the range 10–500 GHz. Our early VSA results (see e.g. Scott et al. 2003; Taylor et al. 2003) were based on a brightness temperature $T_{\rm J} = 152 \pm 5$ K at 32 GHz, extrapolated to 33/34.1 GHz using $\beta = -2.24 \pm 0.1$, from direct measurements (Mason et al. 1999). The VSA calibration is now expressed in terms of the *WMAP* spectrum of Jupiter which is tied to the CMB dipole temperature. At 33 GHz, the most recent *WMAP* value is $T_{\rm J} = 146.6 \pm 0.75$ K (Hill et al. 2008).[2] The ultimate absolute precision of our adopted intensity scale is therefore ≈ 0.5 per cent. Of course we can, in principle, measure relative flux densities/brightness temperatures more accurately than this.

Accurate determination of relative intensities of sources is made from the daily calibration observations and includes data from both the compact and the extended VSA configurations. Longer term flux density or brightness temperature variability measurements are possible from the observations which extend from 2000 September to 2004 October.

The brightness temperature spectrum of Jupiter is shown between 0.1 and 200 GHz in Fig. 1. The broad depression at around 20 GHz is believed to be due to molecular absorption by ammonia. Fig. 1 also shows this part of the spectrum in more detail mainly delineated by the accurate *WMAP* points (Page et al. 2003). The best-fitting temperature spectral index at 33 GHz is $\beta = +0.248 \pm .004$. Models for the Jupiter spectrum by Gulkis, Klein & Poynter (1974) and Winter (1964) give an indication of the expected shape in this frequency range, although neither of them is a good fit over this range.

3.4 The atmospheric contribution

The major effect of the atmosphere on the calibration process in the VSA is its variable contribution to the total system noise which is subject to the AGC. The second smaller contribution is the absorption of source radiation on its passage through the atmosphere to the antenna. Both effects vary with the cosecant of the elevation. A detailed discussion of the atmospheric contribution is given separately by Davies et al. (in preparation).

The AGC system gives a reduction of the astronomical signal relative to the zenith value by a factor

$$\begin{aligned} f_{\rm l} &= \left[T_{\rm R} + T_{{\rm atm}(z)}\right] / \left[T_{\rm R} + T_{{\rm atm}(E)}\right] \\ &= 1/\{1 + \left[T_{{\rm atm}(z)}({\rm cosec}\,E - 1)/(T_{\rm R} + T_{{\rm atm}(z)})\right]\}, \end{aligned} \quad (1)$$

where $T_{\rm R}$ is the receiver noise plus cosmic background and $T_{{\rm atm}(z)}$ and $T_{{\rm atm}(E)}$ are the atmospheric emission at the zenith and at elevation E, respectively. For an average total set noise at the zenith of

[2] It is of interest to note that the previous *WMAP* value (Page et al. 2003) is identical to the new one (Hill et al. 2008) but with a larger error (146.6 $\pm$ 2.0 K) due to beam uncertainties. This led the CBI group (Readhead et al. 2004) to use a weighted estimate between the Mason et al. (1999) and earlier *WMAP* values, obtaining $T_{\rm J} = 147.3 \pm 1.8$ K at 32 GHz.

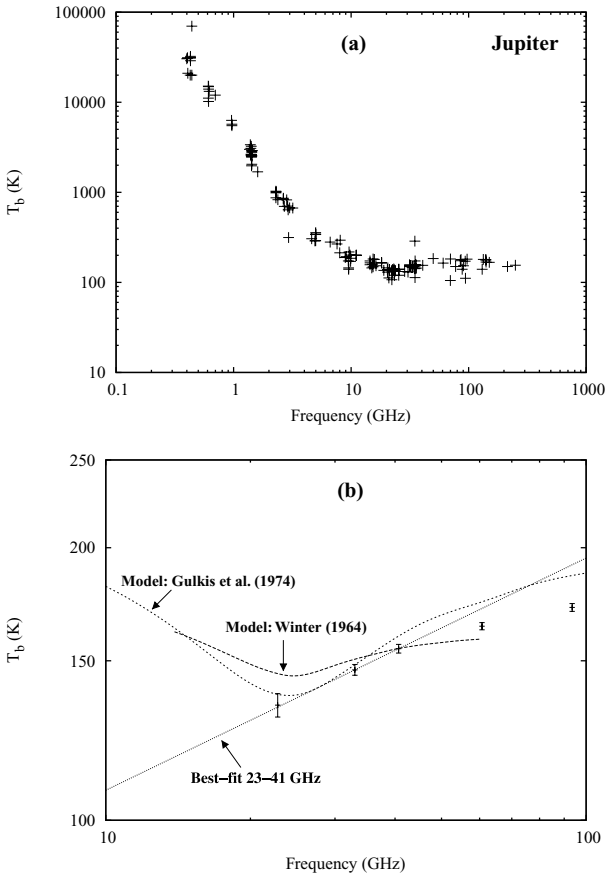

Figure 1. The brightness temperature spectrum of Jupiter. (a) The spectrum covering 0.1–300 GHz from published data; cyclotron emission dominates the lower frequencies and thermal emission the higher frequencies. (b) The spectrum centred around 30 GHz showing the accurate observations from *WMAP* (Page et al. 2003). Models by Gulkis et al. (1974) and Winter (1964) show the effect of ammonia absorption. For the model of Winter (1964), we used values of $T_c = 168$ K and $P_c = 2$ atm.

$T_R + T_{atm(z)} = 35$ K applicable to the VSA antennas and $T_{atm(z)} = 7.5$ K, we obtain

$$f_1 \approx 1 - 0.23(\mathrm{cosec}E - 1), \tag{2}$$

comprising 6.5 K of O_2 emission and 1.0 K water vapour emission, equivalent to 3-mm precipitable water vapour. A similar factor relating the intensity of the astronomical signal arriving at the antenna from an elevation E to that which it would have been at the zenith is

$$\begin{aligned} f_2 &= [\mathrm{e}^{-\tau(E)}]/[\mathrm{e}^{-\tau(z)}] \\ &= 1 - \tau(z)(\mathrm{cosec}E - 1). \end{aligned} \tag{3}$$

For the relevant model atmosphere above Izaña the atmospheric temperature is 260 K, so with $T_{atm(z)} = 7.5$ K,

$$f_2 = 1 - 0.028(\mathrm{cosec}E - 1). \tag{4}$$

The final correction to the source observations for the atmosphere, to first order in (cosec $E - 1$), is

$$f = f_1 f_2 = 1 - 0.26(\mathrm{cosec}E - 1). \tag{5}$$

Since the VSA is restricted to elevations above 50°, the corrections are less than 7 per cent and the approximations in the expressions for f, f_1 and f_2 are valid. In each pair of observations for a flux density comparison, each source is corrected for elevation as in equation (5) and the source ratio corrected to the zenith is obtained.

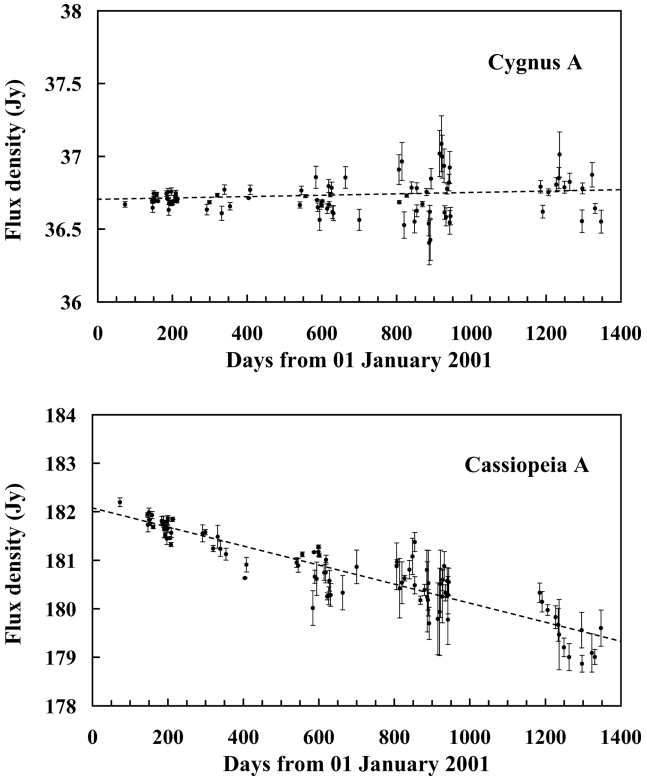

Figure 2. VSA flux density measurements of Cyg A and Cas A calibrated by Jupiter over the period 2001 March 13 to 2004 August 9. The solid lines are least-squares fits to the data.

A convincing demonstration can be made of this calibration technique. The quality of the data corrected as described above can be assessed by intercomparing the three calibrators Jupiter, Cas A and Cyg A, all observed near transit and spread over the period 2002–04. Fig. 2 shows plots of the observed flux density of Cyg A and Cas A using Jupiter as a calibrator. A similar plot for Tau A is given in Fig. 9 below. The daily scatter in the fluxes measured relative to Jupiter is seen to be <1 per cent. The level of thermal noise in a typical daily measurement is ∼0.1 Jy while the daily scatter is ∼1–2 Jy, thus the variations are dominated by the atmosphere. In the case of Cyg A and Cas A, the time difference between the source and Jupiter observation can be as large as 12 h. For Tau A, where the time difference is smaller (<6 h) over this period, the scatter was <0.5 per cent.

Since the main contributor to the scatter is atmospheric water vapour emission, the 1 per cent scatter corresponds to 1 per cent of set noise within the AGC system, which is 0.35 K. At 33 GHz this temperature scatter corresponds to 1 mm precipitable water vapour (Danese & Partridge 1989). Some of the implications of this high level of stability in the atmosphere are included in the discussion of individual sources in Sections 4.1–4.3.

4 DERIVED SOURCE PARAMETERS

We now derive the flux density and/or brightness temperature of our calibration sources at 33.0 GHz relative to Jupiter.

Since our results are most useful to the community working in the ∼10 GHz wide band around 33 GHz, we have derived a spectral

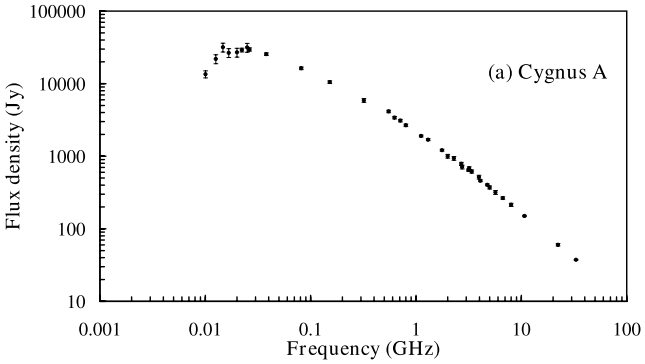

Figure 3. The flux density spectrum of Cyg A from 10 MHz to 100 GHz; the low-frequency turnover is due to Galactic free–free absorption.

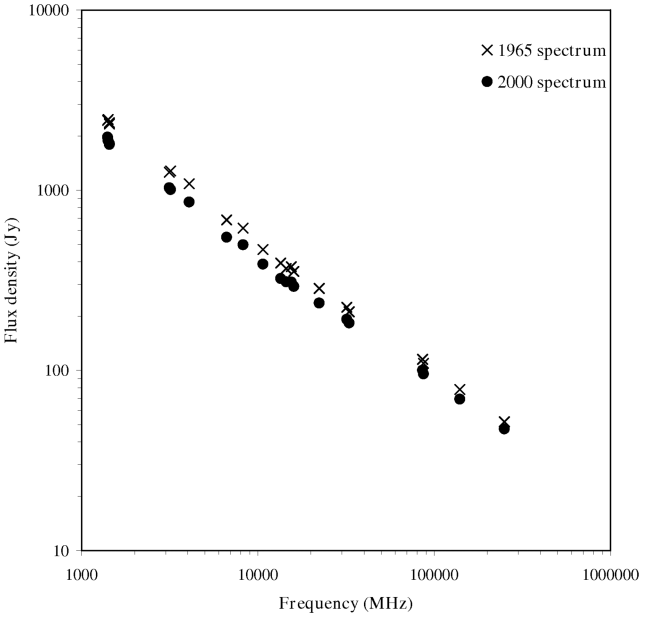

Figure 4. The spectrum of Cas A for the epochs 1965 (crosses) and 2000 (filled circles) calculated from published data with the secular decreases applied appropriate to each frequency (see Section 4.2.3).

index for that range from flux densities in the literature (plus our new determinations). The brightness temperature spectrum of Jupiter has already been discussed in Section 3.3. We extrapolated all the VSA data to a common frequency of 33 GHz using the spectral indices derived from the literature.

For several of the sources in our study, data are available for time-spans between 1 and 4 yr. These accurate data are used to investigate source variability at high precision.

4.1 Cygnus A

Cyg A is a radio source associated with a double galaxy at a redshift of $z = 0.056$ containing a central core and hotspots at the outer ends of diffuse radio lobes. The overall extent is 2.1 arcmin and is effectively unresolved in the compact and extended VSA arrays. No variability has ever been reported for Cyg A at any wavelength.

The radio spectrum of the integrated emission of Cyg A taken from literature is shown in Fig. 3. There are several changes of slope in the spectrum over the frequency range 0.1–100 GHz; one is at ∼0.5 GHz and another is at ∼3 GHz. The slope of the section 5–100 GHz, which includes 33 GHz, is -1.208 ± 0.017. We recommend this as the spectral index at 33 GHz. This value may be compared with -1.244 ± 0.014 given in table 3 of Baars et al. (1977) at similar frequencies.

Observations of the calibration sources Cyg A, Cas A and Jupiter were analysed for the period 2001 March 14 to 2004 4 May. The flux density of Cyg A calibrated by Jupiter (assumed to have a brightness temperature of 146.6 K at 33 GHz) over this period is shown in Fig. 2. In this period the right ascension (RA) of Jupiter ranged from RA = 08 to 12 h so observations were typically separated by 8–12 h. The 1 per cent scatter in the derived flux density of Cyg A was due to the atmosphere (mainly water vapour) over this time range. The mean flux density at 33 GHz was found to be 36.4 ± 0.2 Jy.

These data can also be used to probe the long-term stability of the radio emission from Cyg A and Jupiter at 33 GHz. A fit to the data shows that the flux density ratio of Cyg A and Jupiter increases by 0.043 ± 0.039 per cent yr^{-1}. Accordingly we conclude that the relative radio emission changed by ≤ 0.1 per cent yr^{-1} over the period 2001 March to 2004 May.

4.2 Cassiopeia A

Cas A is a 330-yr-old shell-type SNR of 5 arcmin diameter. Baars et al. (1977) give its spectral index between 0.3 and 31 GHz as $\alpha = -0.792 \pm 0.007$ in 1965 and $\alpha = -0.770 \pm 0.007$ in 1980. Radio imaging shows multiple hotspots with spectral indices between -0.65 and -0.90 (see e.g. Anderson & Rudnick 1996) embedded in extended structure. Steeper spectra are associated with features thought to be bowshocks and with features outside the main radio ring; flatter spectra are found in the ring and in bright features within it which may account for its slow but measurable decrease in flux density with time at a rate which is thought to vary with frequency. These are important considerations when using Cas A as a calibrator.

4.2.1 The Cas A spectrum

Fig. 4 shows the spectrum of Cas A taken from published data over the frequency range 1.0–100 GHz with the flux densities corrected to the years 1965 and 2000 using the recipe given in Section 4.2.3 and listed in Table 2. The spectrum over this large frequency range shows a flattening of the spectral index above 15 GHz not detected in earlier data; this flattening is seen in both the 1965 and 2000 data. In 1965 $\alpha = -0.795 \pm 0.12$ at $\nu < 15$ GHz and $\alpha = -0.725 \pm 0.013$ at $\nu > 15$ GHz. For the 2000 data $\alpha = -0.767 \pm 0.018$ at $\nu < 15$ GHz and $\alpha = -0.663 \pm 0.012$ at $\nu > 15$ GHz. An appropriate spectral index at 33 GHz at the present epoch would appear to be $\alpha = -0.69 \pm 0.02$.

4.2.2 VSA measurements of Cas A

With the resolution of 17 and 11 arcmin for the compact and extended forms of the VSA, Cas A will show significant resolution effects in a project which aims for an accuracy of better than 1 per cent. Accordingly, a correction was applied in the analysis procedure which scaled the visibilities on each baseline. The 5-GHz map from the VLA was used for this purpose. In view of the differing spectral indices within Cas A, it was necessary to confirm that the 5-GHz model was applicable to our 33-GHz observations.

Table 2. Cassiopeia A flux density for epochs 1965 and 2000.

Frequency (GHz)	S_{1965} (Jy)	S_{2000} (Jy)	Secular decrease (per cent yr^{-1})
1.405	2439 ± 50	1970 ± 50	0.67
1.415	2470 ± 50	1885 ± 40	0.67
1.44	2328 ± 50	1793 ± 40	0.66
1.44	2367 ± 20	1813 ± 55	0.66
3.15	1258 ± 38	1030 ± 30	0.62
3.2	1279 ± 58	1008 ± 45	0.61
4.08	1084 ± 26	860 ± 20	0.59
6.66	684 ± 20	548 ± 16	0.57
8.25	615 ± 22	497 ± 18	0.55
10.7	468 ± 0	388 ± 0	0.54
13.49	394 ± 13	323 ± 11	0.53
14.5	367 ± 10	310 ± 9	0.52
15.5	376 ± 18	309 ± 15	0.51
16	354 ± 11	292 ± 9	0.51
22.28	285 ± 10	236 ± 9	0.49
32	224 ± 6	192 ± 5	0.47
33	211 ± 5	183 ± 5	0.47
86	115 ± 4	100 ± 4	0.41
87	109.4±0	95.4±0	0.41
140	78.3±7	69.1±6.2	0.38
250	51.8±5.6	47.2±5.3	0.36

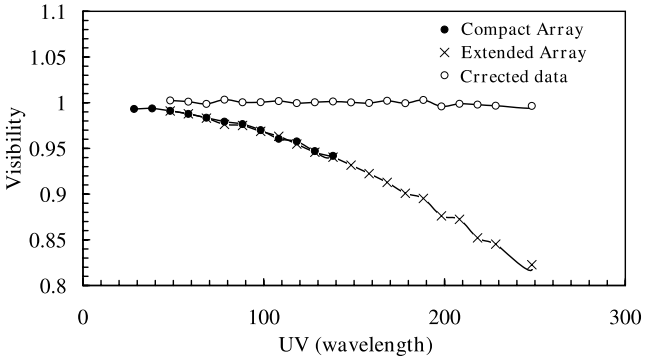

Figure 5. The visibility amplitude of Cas A as a function of VSA baseline length measured in wavelengths. The crosses show the visibilities measured with the extended array; the filled circles show the compact array. The open circles are the visibilities corrected to a 5-GHz observed map of Cas A; this correction brings the visibility to within 1 per cent of unity.

Fig. 5, which plots the visibility amplitude of Cas A versus the baseline length, shows the results of this investigation. It can be seen that the normalized visibility after correction with the model is unity within 1 per cent across the baseline range 20–250 λ. The compact and extended VSA data sets overlap at a precision of better than 0.5 per cent in the baseline range 50–130 λ. The correction model is thus adequate for our purpose. Fig. 2(b) shows the flux density of Cas A measured over the period 2001 March 13 to 2004 August 9. Each point is the average of the flux densities measured relative to Cyg A and Jupiter. The secular decrease in the flux density of Cas A is clearly seen. No seasonal effects are evident in the data as the three sources move from day to night. Moreover the data for the compact array (2000 March to 2001 May) are entirely consistent with those from the extended array; no step is seen in the plot around 2001 May. A linear fit to the data of Fig. 2(b) gives a flux density for Cas A on the adopted Jupiter scale of 182.02 ± 0.07 Jy in 2001 January. The linear rate of decrease over the period 2001 March to 2004 August is given by

$$\frac{\mathrm{d}S}{S\mathrm{d}t} = -0.394 \pm 0.019 \mathrm{percentyr}^{-1}. \quad (6)$$

Table 3. Secular decrease of Cas A as a function of frequency.

Frequency (GHz)	Epoch	Decrease (per cent yr^{-1})
0.038	1955–87	0.8 ± 0.08
0.0815	1949–69	1.29 ± 0.08
0.0815	1949–89	0.92 ± 0.16
0.0815	1965–89	0.63 ± 0.06
0.1025	1977–92	0.80 ± 0.12
0.927	1977–96	0.73 ± 0.05
0.950	1964—72	0.85 ± 0.05
1.405	1965–99	0.62 ± 0.12
1.420	1957–76	0.89 ± 0.02
1.420	1957–71	0.89 ± 0.12
3.000	1961–72	0.92 ± 0.15
3.060	1961–71	1.04 ± 0.21
7.800	1963–74	0.7 ± 0.1
9.400	1961–71	0.63 ± 0.12
15.500	1965–95	0.6 ± 0.06
33.000	2001–04	0.39 ± 0.02

4.2.3 Secular decrease in flux density of Cas A

The current estimate of the secular decrease in the flux density of Cas A at 33 GHz obtained over a 3.5 yr period in the present decade is the most accurate of any epoch. Scott, Shakeshaft & Smith (1969) at 81.5 MHz covering the two decades 1949–69 found a value of 1.29 ± 0.08 per cent yr^{-1}. Using more recent data at 81.5 MHz, Hook, Duffett-Smith & Shakeshaft (1992) found a lower value rate of decrease between 1949 and 1989.7 of 0.92 ± 0.16 per cent yr^{-1}.

We now re-examine the data available relating to the variability of Cas A as a function of both epoch and frequency. The data between 1949 and 1976 in the frequency range 81.5 MHz to 9.4 GHz indicated a secular decrease of flux density estimated by Baars et al. (1977) to be frequency dependent and given by the relation

$$\frac{\mathrm{d}S}{S\mathrm{d}t} = 0.97(\pm0.04) - 0.30(\pm0.04)\log(\nu/\mathrm{GHz})\,\mathrm{per\,cent\,yr}^{-1}. \quad (7)$$

The most accurate data currently available cover the frequency range 38 MHz to 33 GHz and the period 1949–2004 is given in Table 3.

Fig. 6 shows the data from Table 3 divided into two epochs. The filled circles show the secular decrease from ∼1950 to 1970 while the crosses show the decrease from ∼1970 to 1990/2000. It is clearly evident that the earlier data show higher (∼50 per cent) secular decrease than the later data. The data from 1970 to 1990/2000 indicate a secular decrease of

$$\frac{\mathrm{d}S}{S\mathrm{d}t} = 0.68(\pm0.04) - 0.15(\pm0.04)\log(\nu/\mathrm{GHz})\,\mathrm{per\,cent\,yr}^{-1}. \quad (8)$$

The material available is not sufficient to show whether the fall in the secular rate is linear with time or not (as proposed for the 81.5-MHz data by Hook et al. 1992). Apart from the current (2001–04) 33-GHz result the values given by equation (6) may be an upper limit to the secular variation of Cas A at the present epoch. The

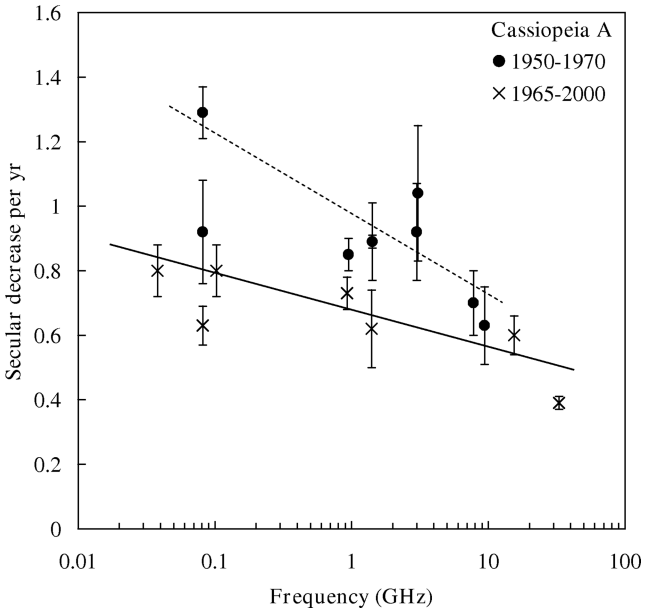

Figure 6. The secular decrease in the flux density of Cas A as a function of frequency for two epochs, 1950–70 (filled circles) and 1965–2000 (crosses). The lines are least-squares fits to the data at the two epochs.

secular decrease of Cas A will be discussed further in a related paper (Lancaster et al., in preparation).

A frequency-dependent secular variation has implications at the present epoch for the spectrum of Cas A. We can apply equation (7) to the higher weight data from table 2 of Baars et al. (1977) and more recent data particularly at higher frequencies (Mezger et al. 1986; Liszt & Lucas 1999; Mason et al. 1999; Wright et al. 1999; Reichart & Stephens 2000; this paper) to derive the spectra for 1965 (the Baars et al. epoch) and for 2000 at frequencies from 1 to 250 GHz). The decrease of the secular term with frequency as shown by equation (7) gives a flattening of the spectral index with time. A synchrotron spectral index which flattens with time implies that particle acceleration is continuing in Cas A, presumably at the shock interfaces in the object (see e.g. Reynolds & Ellison 1992).

4.3 Taurus A

The Crab nebula is the filled-centre remnant of the supernova of AD 1054. The central neutron star remains active and replenishes the supply of relativistic electrons in the nebula. There is some evidence for a small secular decrease of the flux density at both radio and optical wavelengths. The present observations lead to a flux density of Tau A at 33 GHz. Since the source is strongly linearly polarized we must determine the polarization in order to use Tau A as a calibrator at 1 per cent accuracy.

4.3.1 The spectrum of Tau A

Baars et al. (1977) found a constant spectral index over the frequency range 1–35 GHz with value of $\alpha = -0.299 \pm 0.009$. More recent data, including higher frequencies up to 350 GHz, are shown in Fig. 7. A constant spectral index of -0.278 ± 0.007 fits the data between 1 and 350 GHz. The expected turndown of the spectrum is beyond this frequency range and is believed to be at 10 THz (Marsden et al. 1984). There is, however, some evidence for a small curvature of the spectrum. We find $\alpha = -0.258 \pm 0.028$ between 22

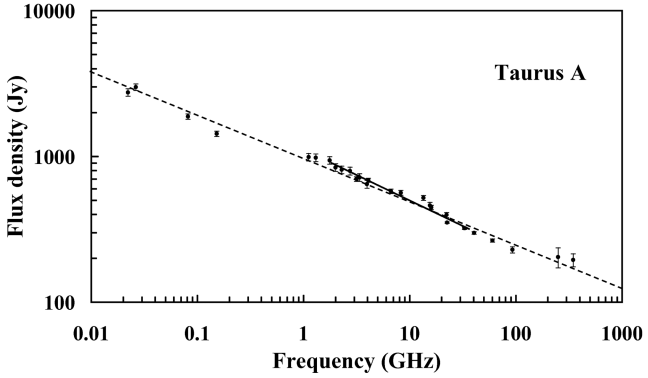

Figure 7. The log–log flux density spectrum of Tau A from 10 MHz to 1000 GHz. A linear slope of $\alpha = -0.278 \pm 0.007$ fits the data from 1 to 350 GHz (dashed line).The slope between 1.8 and 33 GHz (solid line) is $\alpha = -0.351 \pm 0.016$.

and 1800 MHz, $\alpha = -0.351 \pm 0.016$ between 1.8 and 33 GHz and $\alpha = -0.35 \pm 0.03$ between 8 and 347 GHz. Green (2002) gives the spectral index between 1.5 and 347 GHz of individual structures in the nebula to lie in the range -0.31 and -0.34. Similarly Mezger et al. (1986) give a spectral index between images at 10.7 and 250 GHz of $\alpha = -0.30 \pm 0.05$. We adopt $\alpha = -0.32 \pm 0.01$ as an appropriate spectral index at ≈30 GHz, which is consistent with the recent analysis by Macias-Perez et al. (2008).

4.3.2 The VSA observations of Tau A

Care is required when using Tau A as a calibrator in two regards. First, it is an extended source with dimensions of 4×6 arcmin^2 at position angle (PA) $\sim 140^\circ$ and consequently requires a resolution correction when observed with the VSA in both the extended and compact configurations. Secondly, it is some 10 per cent linearly polarized at frequencies of 30 GHz and above and this must be taken into account when observing with linear polarization.

The observed optical polarization of Tau A is 9.2 per cent at PA $= 159\overset{\circ}{.}6$ (Oort & Walraven 1956). The integrated radio polarization increases from 2 per cent at 1.4 GHz to 7 per cent at 5 GHz (Gardner & Davies 1966). The mean Faraday rotation measure (RM) in Tau A is -25 rad m^{-2} with values up to 300 rad m^{-2} in some places. Any RM in this range leads to negligible Faraday rotation (FR) 30 GHz (a wavelength of 1.0 cm) corresponding to a FR $\leq 1^\circ$ (FR $\propto 1/\lambda^2$).

We now consider the VSA data for Tau A.

(i) The linear polarization of Tau A: This can be estimated from long hour angle (HA) tracks of the source, remembering that the VSA is linearly polarized at PA $= 0^\circ$. The maximum HA track for Tau A runs from HA $= -3$ h 00 m to $+3$ h 00 m. The observed data from the extended array on 2001 December 26 calibrated against Cas A (and Jupiter) is shown in Fig. 8 by crosses. This data set is first corrected (circles) for resolution effects of the VSA as for Cas A (Section 4.2.2) using a 1.4-GHz map of Tau A (Bietenholz, Frail & Hester 2001); this model was confirmed by showing that the corrected visibilities were constant with baseline for both the compact and extended VSA configurations in the manner illustrated for Cas A in Fig. 5. The elevation correction for absorption in the atmosphere and the AGC effect on the receivers (0.26 cosec$E$ – see Section 3.4) were then applied giving the true variation of flux density with HA shown as filled circles in Fig. 8. The linearly

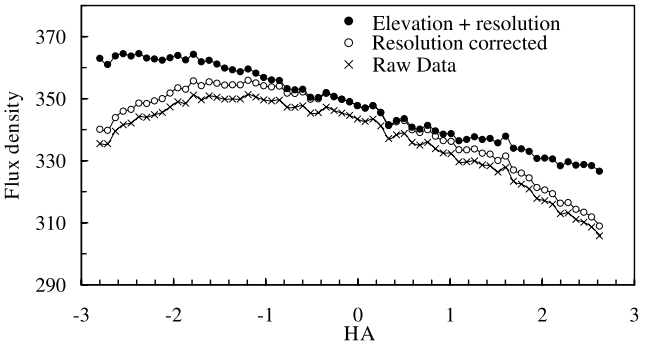

Figure 8. The flux density of Tau A plotted against HA for the observation on 2001 December 26 with the extended array. Crosses show the observed data calibrated against Jupiter; open circles show the data then corrected for resolution affects; filled circles show the data further corrected for elevation (atmospheric absorption and the AGC effect). The resultant sloping HA plot is due to the linear polarization of Tau A.

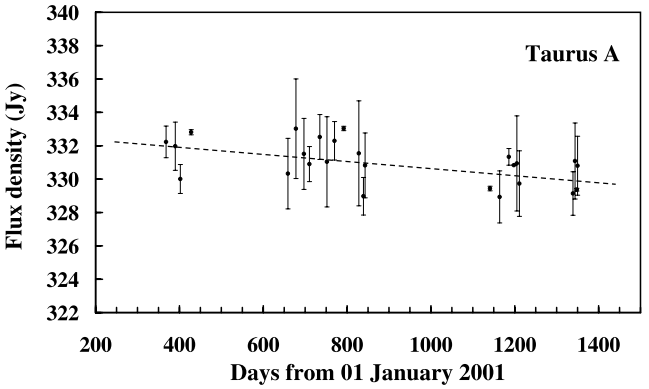

Figure 9. The flux density of Tau A measured relative to Jupiter for the period 2002 January 3 to 2004 September 11. The dashed line is a least-squares fit to the data. The observed secular change is -0.22 ± 0.07 per cent yr^{-1}.

polarized flux density P is then estimated by fitting the corrected data to P cosec $[2(p - \theta)]$, where p is the polarization PA measured east from north and θ is the parallactic angle at the HA of observation. Data from four nights (2001 December 26, 2002 February 09, 2002 October 12 and 2003 January 25) of good weather and analysed as above were averaged to determine the polarization of Tau A. The results of this fitting gave $P = 24.6 \pm 1.6$ Jy corresponding to 7.8 ± 0.6 per cent linear polarization at PA $= 148^\circ \pm 3^\circ$. The errors quoted include the uncertainty in the atmospheric correction.

(ii) The flux density of Tau A at 33 GHz: The total flux density of Tau A is determined by the fitting procedure given in the previous section. The average of the 4 HA scans gives S(Tau A) $= 322 \pm 4$ Jy. The flux density of Tau A at HA $= 0$ h (PA $= 0^\circ$) is 332 ± 4 Jy. A more extensive data set using short calibration tracks running from 2002 January 3 to 2004 September 11 with the extended array gave a more accurate estimate. The individual data points were corrected for resolution and for the atmosphere and are plotted in Fig. 9. The use of Jupiter as the reference for Tau A led to the very low scatter (rms $= 0.4$ per cent) in the data since they were both night-time objects and separated in time by less than 5 h. This data set gives a flux density for Tau A at PA $= 0^\circ$ of 332.8 ± 0.7 Jy on 2001 January 1. The secular decrease of Tau A indicated by Fig. 9 is discussed in the next section.

4.3.3 Secular decay of Tau A

The 950-yr-old nebula is clearly in the decay phase although centrally re-energized from the spindown of its central pulsar. Theoretical models predict a secular decrease of 0.16–0.4 per cent yr^{-1} at radio wavelengths (Reynolds & Chevalier 1984). An extended series of observations at 8.0 GHz over the period 1969–85 by Aller & Reynolds (1985) gave a decrease of 0.167 ± 0.015 per cent yr^{-1}, a value consistent with the theoretical models (an interesting determination of the optical decay of the continuum at 5000 Å using data from 1960 to 2002.2 has been made by Smith (2003) who found a decay of 0.5 ± 0.2 per cent yr^{-1}).

The current 33-GHz observations of Tau A presented in Fig. 9 and described in the previous section give a secular decrease over the period 2002 January to 2004 September of

$$\frac{\mathrm{d}S}{S\mathrm{d}t} = -0.22 \pm 0.07 \,\text{per cent yr}^{-1}. \quad (9)$$

This is very similar to the value obtained by Aller & Reynolds (1985) at 8.0 GHz for the longer but earlier period 1968–85 and is also consistent with the models of Reynolds & Chevalier (1984). A secular decrease of $\sim$0.2 per cent yr^{-1} would seem to be appropriate for the present epoch at 33 GHz.

4.4 NGC 7027

NGC 7027 is young planetary nebula which is optically thick in Lyman continuum and is therefore an ionization-bounded ionized hydrogen region. The radio continuum and optical nebula have dimensions of 12×8 arcsec^2 (Basart & Daub 1987). It is surrounded by a ring of neutral molecular gas and dust some 40 arcsec in diameter possibly extending to 70 arcsec (see e.g. Bieging, Wilner & Thronson 1991; Hoare, Roche & Clegg 1992). The expansion age of NGC 7027 is 1200 yr with an expansion rate of 4.2 ± 0.6 mas yr^{-1} (Masson 1989).

Three factors are of particular interest in the present study. The first is the activity within the nebula; its expansion velocity is 17.5 ± 1.5 km s^{-1} with local gas velocities up to 55 km s^{-1} (Lopez et al. 1998; Cox et al. 2002). These motions may lead to secular variations of radio flux density. The second effect is the clumpiness of the ionized gas in NGC 7027 which results in optically thick knots up to at least 5 GHz (Bains et al. 2003). This determines the frequency range for which an optically thin radio thermal spectrum (at $T_e \approx 14\,000$ K) may be adopted. Thirdly, the dust within and surrounding NGC 7027 may produce anomalous radio emission as in the case of the Helix nebula (Casassus et al. 2004) and LDN 1622 (Casassus et al. 2006). Such emission, which peaks in the range 10–30 GHz (Draine & Lazarian 1998), needs to be considered when discussing the spectrum of NGC 7027.

4.4.1 Spectrum of NGC 7027

The radio spectrum of the integrated emission from NGC 7027 is shown in Fig. 10 from the radio to the far-infrared (FIR). It consists of several components. At radio frequencies the spectrum is due to free–free emission, optically thick at the lower frequencies and optically thin at the higher radio frequencies. The transition to optically thin occurs at $\sim$5–10 GHz in agreement with the observation by Bryce et al. (1997) that the bright north-west knot has an optical depth of $\sim$2.0 at 5 GHz. A fit to the data between 10 and 80 GHz gives an optically thin spectral index of -0.119 ± 0.025. The expected local value of the thermal spectral index for the observed electron temperature (14 000 K) in this frequency range lies

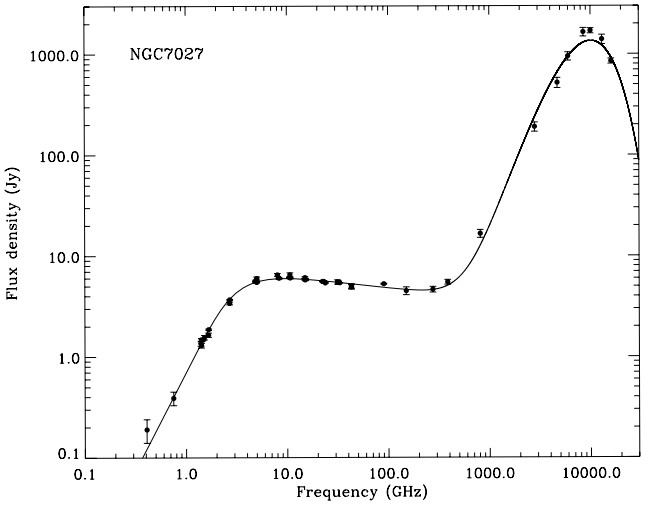

Figure 10. The flux density spectrum of NGC 7027 covering the range 408 MHz to 16 000 GHz using data from the literature. The solid line is a fit consisting of an optically thick and thin free–free spectrum in addition to a single component modified blackbody dust model. At frequencies of ∼30 GHz, the spectrum is dominated by optically thin free–free emission.

between −0.111 (at 10 GHz) and −0.133 (43 GHz) (Dickinson, Davies & Davis 2003).

The FIR emission consists of two components. One is warm (100 K) dust inside the 12 × 8 arcsec^2 ionized hydrogen region and the other is cool (30 K) dust in a neutral gas ring 40 arcsec in diameter surrounding the nebula (Bieging et al. 1991; Hoare et al. 1992). Both these dust components are covered by the observing beamwidth of the VSA and are included in the integrated emission described here.

The question of whether there is significant anomalous radio emission from either or both of the dust components can be addressed. There is no obvious emission with a peaked spectrum of roughly an octave width centred at ≈20 GHz in the spectrum of Fig. 10. For a normal cool dust cloud the expected emission based on the 100-μm (3-THz) flux density would be ≈0.3 Jy (Watson et al. 2005; Casassus et al. 2006; Davies et al. 2006). The emission from a normal H II region (Dickinson et al. 2006, 2007) would be ≈ 0.1 Jy. The latter is more consistent with Fig. 10.

4.4.2 The variability of NGC 7027

The flux densities measured over the period 2002 June to 2003 July are shown in Fig. 11. There is weak evidence for a higher flux density in the six observations before 2002 July 10. After this time the flux density remains constant for the year; a linear fit to the latter data gives an insignificant annual change of -0.31 ± 0.37 per cent yr^{-1}. A fit to the full run of the data gives a decrease of 0.8 ± 0.3 per cent yr^{-1}. The average flux density of NGC 7027 in the period 2002 June to 2003 July is 5.39 ± 0.04 Jy.

The long-term secular variation of NGC 7027 at radio frequencies is often discussed (see e.g. Masson 1989; Ott et al. 1994). A substantial data set covering the frequency range 4.8–43 GHz is available in the literature extending back to 1967. Fig. 12 shows the flux density of NGC 7027 from 1967 to 2003 in two frequency ranges: 4.8–6.6 GHz where free–free self-absorption becomes significant and 8.0–43 GHz where the spectrum is optically thin as can

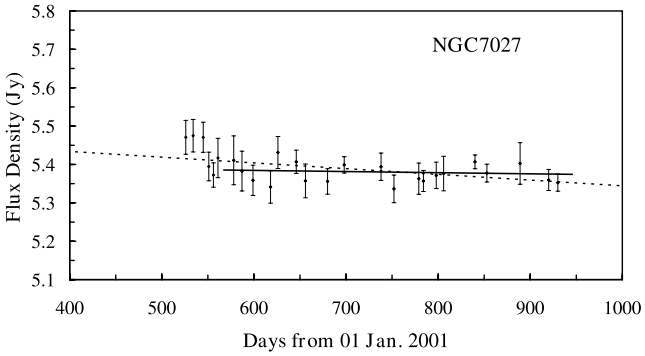

Figure 11. The flux density of NGC 7027 calibrated by Jupiter and Cyg A for the period 2002 June to 2003 July, as measured by the VSA. There is weak evidence for a higher flux density in the first six data points. The annual change for the full data set (dashed line) is -0.8 ± 0.3 per cent yr^{-1}; the change for the data excluding the first six points (solid line) is -0.31 ± 0.37 per cent yr^{-1}.

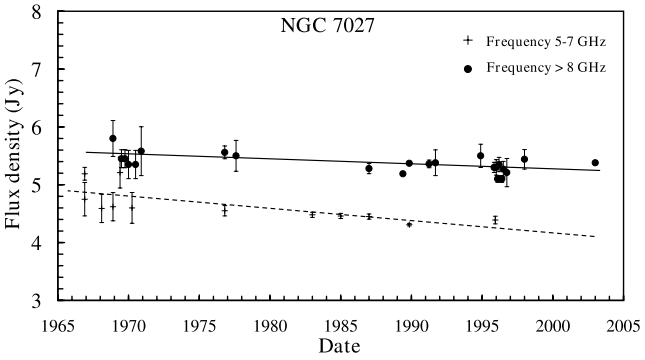

Figure 12. The flux density of NGC 7027 from published data for two frequency ranges over the period 1967–2004 with least-squares fits: (a) solid line and filled circles; optically thin frequencies, 8.0–43 GHz and (b) dashed line and crosses; partially optically thick frequencies, 4.8–6.6 GHz.

be seen in Fig. 10. All flux densities are corrected to a frequency of 33 GHz, assuming an optically thin spectral index $\alpha = -0.12$ as expected theoretically for this frequency range (Dickinson et al. 2003). The 4.8–6.6 GHz flux densities (median frequency 5.2 GHz) are 82 ± 3 per cent of the optically thin frequencies, indicating $\tau = 0.18$ at 5 GHz. Giving each point equal weight, the secular change in the flux density at optically thin frequencies (8.0–43 GHz) is

$$\frac{\mathrm{d}S}{S\mathrm{d}t} = -0.159 \pm 0.043\,\text{per cent yr}^{-1}. \quad (10)$$

At the slightly optically thick frequencies (4.8–6.6 GHz)

$$\frac{\mathrm{d}S}{S\mathrm{d}t} = -0.45 \pm 0.13\,\text{per cent yr}^{-1} \quad (11)$$

when taking all the data. However, discarding the earlier data with larger errors, the secular change from 1975 to 1996 is

$$\frac{\mathrm{d}S}{S\mathrm{d}t} = -0.183 \pm 0.052\,\text{per cent yr}^{-1} \quad (12)$$

in close agreement with the optically thin data. We therefore have consistent results from two independent data sets. On combining the above data, we conclude that for NGC 7027

$$\frac{\mathrm{d}S}{S\mathrm{d}t} = -0.17 \pm 0.03\,\text{per cent yr}^{-1} \quad (13)$$

over the period ∼1970 to the present.

After completion of this work Zijlstra, van Hoof & Perley (2008) published observations made with the VLA at frequencies in the range 1.275–43.34 GHz covering the period 1983–2006. They find that over this shorter period the flux density increases at lower frequencies where the emission is optically thick and decreases at higher (optically thin) frequencies. The turnover occurs between 2 and 4 GHz. Their value of decrease at optically thin frequencies of 0.145 ± 0.005 per cent yr^{-1} is consistent with that of the present study covering data from the 36 yr period to 2003.

4.5 Venus

The radio spectrum of Venus is the result of contributions from different depths in its atmosphere at high frequencies and from the surface at low frequencies. At the surface the temperature is ≈750 K and the pressure ≈90 bar. The millimetric emission arises from the higher atmosphere at $h \approx 80$ km where the effective temperature is 300 K. At intermediate radio frequencies the emission arises from the finite microwave opacity of SO_2 and $H_2\,SO_4$. At 33 GHz where the brightness temperature is ≈460 K the effective altitude of the emission is 35 km; this is the altitude at which space probes recorded a temperature of 460 K and a pressure of ≈5 bar. At altitudes of ∼100 km a strong Venusian diurnal effect has been measured by space probes. We have examined our data to determine whether this diurnal effect extends down to altitudes around 35 km where the 33-GHz emission arises.

For the diameter of Venus, we have adopted the standard values used in the Jet Propulsion Laboratory Ephemeris, which is based on an equatorial radius of 6051.9 km. However, since the 33-GHz emission comes from a height of ≈35 km, the actual brightness temperature averaged over the surface will be 1.2 per cent higher than this.

4.5.1 The spectrum of Venus

Fig. 13(a) shows the radio brightness temperature spectrum of Venus. The low frequencies come from the surface region where the temperature is ∼750 K. The higher GHz frequencies arise in successively higher levels in the Venusian atmosphere where temperatures are lower. The slope of the T_b spectrum at 33 GHz, estimated from a best fit to the range 10–100 GHz, is -0.278 ± 0.026 (the temperature spectral index, β, is related to the flux density spectral index, α, by $\beta = \alpha - 2$).

4.5.2 Brightness temperature variation with illumination

Fig. 14 shows the 33-GHz brightness temperature of Venus as a function of illumination for the period 2002 August to 2004 September. During this period, Venus went through 1.5 Synodic cycles. Data are shown separately for eastern and western illumination, corresponding to times when the Venusian surface was entering or leaving the long period of darkness. No difference is seen between these two phases of illumination of more than 2 K (0.3 per cent). The variation of brightness temperature with illumination suggests a weak increase of temperature with illumination of $+1.5 \pm 1.3$ per cent (6.9 ± 6.0 K) from zero to full illumination.

4.6 Saturn

Saturn is used as a secondary calibrator by the VSA. For accurate measurements the effect of the rings must be taken into account. The rings themselves emit with a brightness temperature of 10–20 K and also block out the emission from the disc of Saturn (see e.g. Janssen & Olsen 1978; Conway 1980; Ulich 1981). As a consequence, the effective brightness temperature of Saturn varies with the tilt angle B (the Saturnicentric latitude of the Earth). We present data for the period 2002 June to 2003 August.

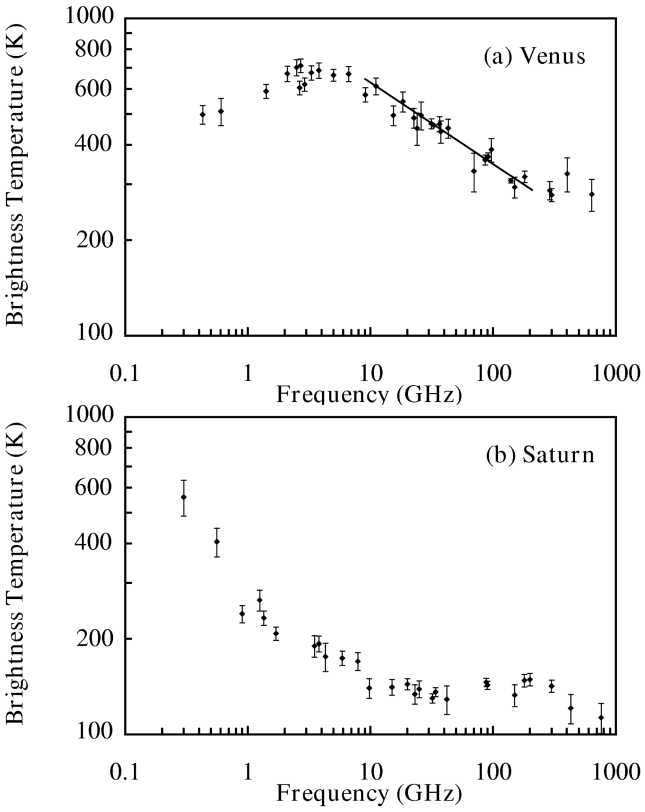

Figure 13. (a) The brightness temperature spectrum of Venus from the literature. The solid line shows the least-squares best-fitting slope between 10 and 100 GHz which gives a T_b spectral index at 33 GHz of -0.278 ± 0.026. (b) The brightness temperature spectrum of Saturn from the literature.

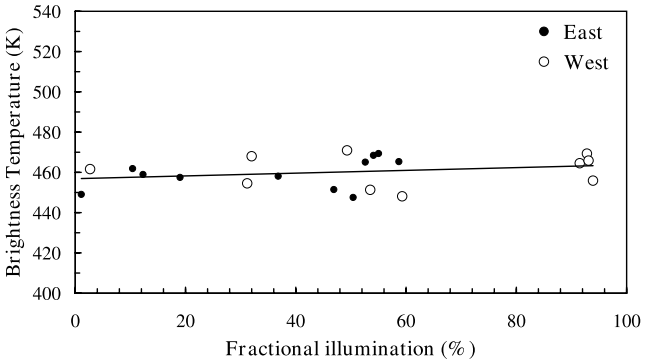

Figure 14. The brightness temperature of Venus plotted as function of illumination for the period 2002 August to 2004 September. Filled circles show eastern illumination (surface entering darkness) and open circles show western illumination (leaving darkness). The solid line is the best linear fit to the data corresponding to $+1.5 \pm 1.4$ per cent change from zero to full illumination.

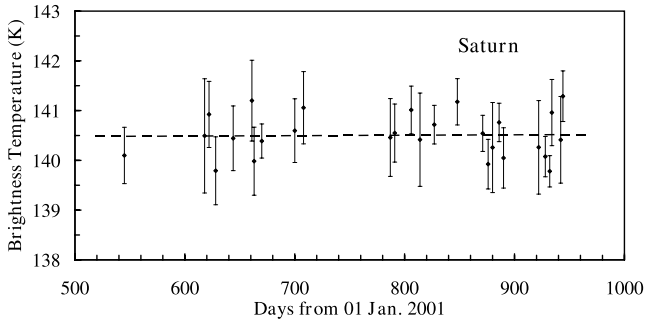

Figure 15. The brightness temperature of Saturn at 33 GHz for the period 2002 June 29 to 2003 August 02. There is no secular variation greater than 0.4 per cent yr^{-1} over this period.

4.6.1 The spectrum of Saturn

The microwave spectrum of Saturn taken from the literature is plotted in Fig. 13(b) in terms of its brightness temperature. There is some uncertainty as to the contribution of the rings to the data presented. Since the ring effect is typically less than 5 per cent, it lies within the error assigned to most data points in Fig. 13(b). The shape of the spectrum is quantitatively similar to that of Jupiter – increasing from ≈130 K at mm wavelengths to 540 K at 94 cm. As in the case of Jupiter there is evidence for the presence of ammonia as the principal source of opacity at radio frequencies with its inversion band at ≈24 GHz. At 30 GHz, the frequency of interest in the present study, the effective temperature spectral index is $\beta = 0.00 \pm 0.05$. At frequencies of 10–43 GHz, $\beta = -0.07 \pm 0.05$, while at 10–200 GHz, $\beta = +0.041 \pm 0.015$.

4.6.2 Secular variation of Saturn at 33 GHz

The VSA programme gave an accurate data set for the integrated flux density of Saturn extending from 2002 June 29 to 2003 August 02. During this period the tilt angle moved between $B = 26^\circ$ and 27° with a quasi-annual period. The brightness temperature is then calculated by assuming that the observed flux density arises from Saturn's disc whose dimensions are given in the Jet Propulsion Laboratory Ephemeris. Fig. 15 is the brightness temperature plot over this period and shows no secular variation greater than 0.4 per cent yr^{-1} at 95 per cent confidence level. Our results indicate that the mean brightness temperature of Saturn (disc plus rings) between 2002 June and 2003 August is 140.50 ± 0.12 K; for the data set the mean tilt angle $B = 26.^\circ5$.

5 CONCLUSION

We have determined the flux density or brightness temperature at 33 GHz of seven sources used by the VSA for calibration; the results are summarized in Tables 4 and 5. This list includes sources widely used for calibration in this frequency range in radio source and CMB studies; they are the strong sources and planets. The high level of reliability of the VSA and the stable atmosphere at the Izaña site have assured accurate relative measurements of these sources. We use Jupiter as the reference standard in this paper and adopt a brightness temperature of 146.6 ± 0.75 K at 33 GHz as determined in the *WMAP* survey (Hill et al. 2008). Any refinement in the future can then be applied to the present results. In order to make our results useful for accurate flux density/brightness temperature measurements in the frequency band around 33 GHz we derive a spectral index from the published data.

Table 4. Secular change in flux density (or brightness temperature) of calibrators relative to Jupiter at 33 GHz (epoch 2001.0).

Radio sources	dS/S dt (per cent yr^{-1})
Cas A	-0.394 ± 0.019
Tau A	-0.22 ± 0.07
NGC 7027[a]	-0.16 ± 0.04
Cyg A	$+0.043 \pm 0.039$
Venus[b]	$+1.5 \pm 1.3$

[a]At optically thin frequencies; see Section 4.4.2. [b]Secular variation of T_b with illumination; see Section 4.5.2.

Table 5. Summary of calibrator flux densities or brightness temperatures at 33 GHz and epoch 2001.0, all relative to an adopted Jupiter $T_b = 146.6$ K.

Radio sources	Flux density (Jy)	Error (Jy)	Spectral index (at 33 GHz)
Cas A	182.0	0.1	-0.69 ± 0.02
Cyg A	36.4	0.2	-1.208 ± 0.017
Tau A[a,b]	322	4	-0.32 ± 0.01
NGC 7027[c]	5.39	0.04	-0.119 ± 0.025
Planets	Brightness temperature (K)	Error (K)	Spectral index (at 33 GHz)
Jupiter	146.6	0.75	$+0.248 \pm 0.004$
Venus	460.3	3.2	-0.278 ± 0.026
Saturn[d]	140.50	0.12	0.00 ± 0.05

[a]Tau A is 7.8 ± 0.6 per cent yr^{-1} linearly polarized at PA $=148^\circ \pm 3^\circ$. [b]Tau A flux density is 332.8 ± 0.7 Jy at PA $= 0^\circ$. [c]Flux density at 2003.0. [d]Flux density at 2003.0; tilt angle B of rings is $26.^\circ5$.

Since we have observations of the calibrators extending over nearly 4 yr, we are able to make an accurate assessment of the calibrator variation over this period. With rms individual comparison measurements of 0.4–1.0 per cent depending on the time separation of the pair of observations, we are sensitive to small secular flux density or brightness temperature variations. A significant secular decrease in flux density was established for Cas A and Tau A over the four-year observing period. By combining our data with historical data in the literature, we have also demonstrated a significant secular decrease for NGC 7027 at optically thin frequencies. Over this period the secular variation of the two sources expected not to vary, Cyg A and Jupiter, was less than 0.1 per cent yr^{-1}. Venus showed a slight (1.5 ± 1.3 per cent) variation with illumination.

ACKNOWLEDGMENTS

We thank the referee, Dayton Jones, for a careful reading of the paper which has led to a number of improvements. YAH thanks the King Abdulaziz City of Science and Technology for support. YAH also thanks His Highness Prince Dr Turki Bin Saud Bin Mohammad Al Saud, the vice president of KACST for the Research institutes, for his personal support. CD acknowledges support from the US Planck Project, which is funded by the NASA Science Mission Directorate.

REFERENCES

Aller H. D., Reynolds S. P., 1985, in Kafatos M. C., Henry R. B. C., eds, Proc., The Crab Nebula and Related Supernova Remnants. Cambridge Univ. Press, Cambridge, p. 75

Anderson M. C., Rudnick L., 1996, ApJ, 456, 234
Baars J. W. M., Genzel R., Pauliny-Toth I. I. K., Witzel A., 1977, A&A, 61, 99
Bains I., Bryce M., Mellema G., Redman M. P., Thomasson P., 2003, MNRAS, 340, 381
Basart J. P., Daub C. T., 1987, ApJ, 317, 412
Bieging J. H., Wilner D., Thronson H. A. Jr, 1991, ApJ, 379, 271
Bietenholz M. F., Frail D. A., Hester J. J., 2001, ApJ, 560, 254
Bryce M., Pedlar A., Muxlow T., Thomasson P., Mellema G., 1997, MNRAS, 284, 815
Casassus S., Readhead A. C. S., Pearson T. J., Nyman L.-A., Shepherd M. C., Bronfman L., 2004, ApJ, 603, 599
Casassus S., Cabrera G. F., Forster F., Pearson T. J., Readhead A. C. S., Dickinson C., 2006, ApJ, 639, 951
Conway R., 1980, MNRAS, 190, 169
Cox P., Huggins P. J., Maillard J.-P., Habart E., Morisset C., Bachiller R., Forveille T., 2002, A&A, 384, 603
Danese L., Partridge R. B., 1989, ApJ, 342, 604
Davies R. D. et al., 1996, MNRAS, 278, 883
Davies R. D., Dickinson C., Banday A. J., Jaffe T. R., Górski K. M., Davis R. J., 2006, MNRAS, 370, 1125
Dickinson C., Davies R. D., Davis R. J., 2003, MNRAS, 341, 369
Dickinson C. et al., 2004, MNRAS, 353, 732
Dickinson C., Casassus S., Pineda J. L., Pearson T. J., Readhead A. C. S., Davies R. D., 2006, ApJ, 643, L111
Dickinson C., Davies R. D., Bronfman L., Casassus S., Davis R. J., Pearson T. J., Readhead A. C. S., Wilkinson P. N., 2007, MNRAS, 379, 297
Draine B. T., Lazarian A., 1998, ApJ, 508, 157
Gardner F. F., Davies R. D., 1966, Aust. J. Phys., 19, 441
Genova-Santos R. et al., 2008, MNRAS, submitted (arXiv:0804.0199)
Green D. A., 2002, in Slane P. O., Gaensler B. M., eds, ASP Conf. Ser. Vol. 271, Neutron Stars in Supernova Remnants. Astron. Soc. Pac., San Francisco, p. 153
Gulkis S., Klein M. J., Poynter R. L., 1974, in Woszczyk A., Iwaniszewska C., eds, Proc. IAU Symp. 65, Exploration of the Planetary System. Reidel, Dordrecht, p. 367
Hill R. S. et al., 2008, ApJS, submitted (arXiv:0803.0570)
Hinshaw G. et al., 2008, preprint (arXiv:0803.0732)
Hoare M. G., Roche P. F., Clegg R. E. S., 1992, MNRAS, 258, 257
Hook I. M., Duffett-Smith P. J., Shakeshaft J. R., 1992, A&A, 255, 285
Janssen M. A., Olsen E. T., 1978, Icarus, 33, 263
Liszt H., Lucas R., 1999, A&A, 347, 258
Lopez J. A., Meaburn J., Bryce M., Holloway A. J., 1998, ApJ, 493, 803
Macias-Perez J. F., Mayet F., Desert F. X., Aumont J., 2008, preprint (arXiv:0802.0412)
Maisinger K., Hobson M. P., Saunders R. D. E., Grainge K. J. B., 2003, MNRAS, 345, 800
Marsden P. L., Gillett F. C., Jennings R. E., Emerson J. P., de Jong T., Olnon F. M., 1984, ApJ, 278, L29
Mason B. S., Leitch E. M., Myers S. T., Cartwright J. K., Readhead A. C. S., 1999, AJ, 118, 2908
Masson C. R., 1989, ApJ, 336, 294
Mezger P. G., Tuffs R. J., Chini R., Kreysa E., Gemuend H.-P., 1986, A&A, 167, 145
Oort J. H., Walraven T., 1956, Bull. Astron. Inst. Netherlands, 12, 285
Ott M., Witzel A., Quirrenbach A., Krichbaum T. P., Standke K. J., Schalinski C. J., Hummel C. A., 1994, A&A, 284, 331
Page L. et al., 2003, ApJS, 148, 39
Readhead A. C. S. et al., 2004, ApJ, 609, 498
Reichart D. E., Stephens A. W., 2000, ApJ, 537, 904
Reynolds S. P., Chevalier R. A., 1984, ApJ, 278, 630
Reynolds S. P., Ellison D. C., 1992, in Holt S. S., Neff S. G., Urry C. M., eds, AIP Conf. Ser. Vol. 254, Testing the AGN Paradigm. Am. Inst. Phys., New York, p. 455
Scott P. F., Shakeshaft J. R., Smith M. A., 1969, Nat, 223, 1139
Scott P. F. et al., 2003, MNRAS, 341, 1076
Smith N., 2003, MNRAS, 346, 885
Taylor A. C. et al., 2003, MNRAS, 341, 1066
Ulich B. L., 1981, AJ, 86, 1619
Watson R. A. et al., 2003, MNRAS, 341, 1057
Watson R. A., Rebolo R., Rubiño-Martín J. A., Hildebrandt S., Gutiérrez C. M., Fernández-Cerezo S., Hoyland R. J., Battistelli E. S., 2005, ApJ, 624, L89
Winter S., 1964, Technical Note, Series 5, Issue 23, Space Sci Lab., UC Berkeley
Wright M., Dickel J., Koralesky B., Rudnick L., 1999, ApJ, 518, 284
Zijlstra A. A., van Hoof P. A. M., Perley R. A., 2008, ApJ, submitted (arXiv:0801.3327)

This paper has been typeset from a TEX/LATEX file prepared by the author.